AGU PUBLICATIONS

Geophysical Research Letters

RESEARCH LETTER
10.1002/2014GL060691

Key Points:
- A slip weakening behavior is systematically observed during the SSE
- The constitutive relations remain unchanged before and after a large earthquake
- Constraints are placed on the rate and state law parameters

Supporting Information:
- Readme
- Figure S1
- Figure S2
- Figure S3
- Figure S4
- Figure S5

Correspondence to:
J. Maury,
J.Maury@brgm.fr

Citation:
Maury, J., H. Aochi, and M. Radiguet (2014), Fault constitutive relations inferred from the 2009–2010 slow slip event in Guerrero, Mexico, *Geophys. Res. Lett.*, *41*, doi:10.1002/2014GL060691.

Received 28 MAY 2014
Accepted 11 JUL 2014
Accepted article online 15 JUL 2014

Fault constitutive relations inferred from the 2009-2010 slow slip event in Guerrero, Mexico

Julie Maury[1], Hideo Aochi[1], and Mathilde Radiguet[2]

[1]Risk and prevention division, BRGM, Orleans, France, [2]EPFL, Lausanne, Switzerland

Abstract The spatiotemporal evolution of stress state is analyzed during the 2009–2010 Slow Slip Event (SSE) of Guerrero, Mexico, based on the kinematic inversion results and using an integral expression for stress changes. A linear slip weakening behavior is generally observed during the SSE with an average slope of -0.5 ± 0.2 MPa/m regardless the perturbation due to the 27 February 2010 $M_w = 8.8$ Maule, Chile earthquake. This slope remains unchanged before and after the Maule earthquake. However, for some area, the friction behavior changes from slip hardening to slip weakening following the Maule earthquake. The complex trajectory between shear stress and slip velocity is fitted with a rate- and state friction law through an inversion. The direct (rate) effect (parameter *A*) is found to be very small, lower by an order of magnitude than the evolutional (state) effect (parameter *B*). The characteristic length *L* is obtained as 5 cm on average.

1. Introduction

Various Slow Slip Events (SSEs) have been recently discovered around the world, especially through GPS measurements. SSEs are characterized [*Peng and Gomberg*, 2010] by long durations, from a few days (short-term SSEs in Japan and Costa Rica) to more than a year (Mexico), and an absence of seismic wave emissions. Their equivalent magnitude can exceed 7 (M_w7 in New Zealand, M_w7.2 in Alaska, and M_w7.5 in Guerrero, Mexico) raising the question about the influence of SSEs on the seismic cycle. SSEs seemingly occur in the transition zone just below the seismogenic zone of the subduction interface, in an area of low effective normal stress [*Beroza and Ide*, 2009]. As the impact on the seismogenic zone depends on the spatiotemporal extension of the SSEs and on the frictional properties, a better understanding of the constitutive friction laws during the SSEs is important.

In addition to the observational efforts in the last decade, SSEs have also been studied through numerical simulations to explain their time scale, slip amount, and location in depth. These studies usually adopt the rate- and state-dependent friction laws [e.g., *Shibazaki and Shimamoto*, 2007; *Liu and Rice*, 2005], as the slip velocity is quite low ($\sim 10^{-8}$ m/s). The so-called aging law [*Dieterich*, 1979; *Marone*, 1998] gives the following evolution in shear stress τ:

$$\tau = \left[\mu_* + a.\ln\left(\frac{V}{V_*}\right) + b.\ln\left(\frac{V_*\theta}{L}\right)\right] * \sigma_n \text{ and}$$
$$\frac{\mathrm{d}\theta}{\mathrm{d}t} = 1 - \frac{V\theta}{L} \quad (1)$$

where V is the slip rate, a and b are experimentally determined parameters (coefficients for "rate" and "state" effects, respectively), L is a characteristic distance, μ_* is the friction coefficient at a reference slip rate V_*, and σ_n is the applied effective normal stress. This law results in a velocity weakening or strengthening behavior at steady state depending on the sign of $(b - a)$, which might vary with temperature and therefore with depth [*Marone*, 1998]. The characterization of the frictional parameters (L, a, and b) is crucial to model the fault behavior. Therefore, this study aims to analyze the spatiotemporal stress evolution of the SSEs, based on a kinematic slip model, without imposing any friction parameter.

Mexico (Guerrero) is our target zone. In the Guerrero area, the Cocos plate is subducting under the North American plate (Figure 1) at a rate of approximately 5.5 cm/year (Nuvel 1A model). A seismic gap of 200 km length exists where no large subduction earthquake has occurred since 1911. It is in this same area that SSEs have been detected. SSEs occur approximately every 4 years and produce surface displacement of a few centimeters over 1 year. They have an equivalent magnitude of 7.5 [*Radiguet et al.*, 2012]. This paper focuses on the SSE occurrence of 2009–2010, because the spatiotemporal slip history has been analyzed

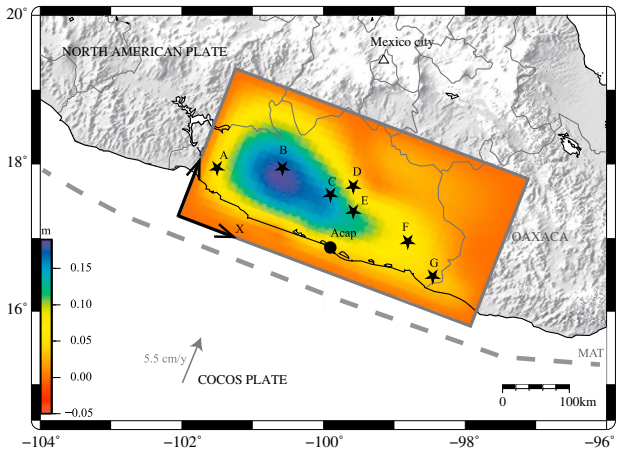

Figure 1. Slip distribution of the 2009–2010 SSE in Guerrero, Mexico [after *Radiguet et al.*, 2012]. The orientations of the axes (strike and dip) in Figure 2 are shown by the thick black arrows. The stars indicate the locations of the subfaults plotted in Figures 3 and 4. The grey arrow indicates the direction of motion between the Cocos plate and the North American plate. Acap: Acapulco. MAT: Middle American Trench.

[*Radiguet*, 2011] and because this SSE has a complex spatiotemporal pattern, with two slip phases. After the first subevent seems to have finished naturally, the second one is most likely triggered by the stress perturbation produced by the 27 February 2010 M_w8.8 Maule, Chile, earthquake [*Zigone et al.*, 2012]. This unique occurrence allows us to study how the stresses and the fault constitutive relation change before and after an external stress perturbation.

2. Model and Method

The detailed spatial and temporal evolution of the 2009–2010 SSE is obtained through a kinematic inversion based on continuous GPS time series from 15 stations (see Figure S1 to S3 in the supporting information). *Radiguet* [2011] use the principal component analysis inversion method initially developed by *Kositsky and Avouac* [2010] to obtain the slip history on the subduction fault plane, which is divided into 720 subfaults of 12.5 km × 13 km (Figure 1). This method has the advantage of imposing no form of source time function, but the solution is regularized to avoid spurious slip. The analysis of this paper is based on this solution (see Figure 2 (first column)).

We calculate the spatiotemporal evolution of stresses from the slip history based on the theory of linear elasticity, as proposed for regular earthquakes (coseismic dynamic rupture propagation) by *Ide and Takeo* [1997]. Following the representation theorem, the stress change τ in the medium is calculated as the convolution of the causal fault slip u and the medium's response function (kernel) G over the slipping area Σ [see *Tada et al.*, 2000, equation (35)]:

$$\tau(\vec{x}) = \int G(\vec{x} - \vec{\xi})u(\vec{\xi})\mathrm{d}\Sigma \tag{2}$$

We compute the analytical Green's function in a homogeneous, infinite elastic medium in the expression of G for equation (2). The u in equation (2) is the cumulative fault slip from the beginning of the analysis (namely, 22 May 2009). The calculated shear stress is then the stress change during the period for the given fault slip, beginning from the initial stress level ($\tau = 0$ at $t = 0$). The stress evolution is calculated every 10 days by temporally interpolating the original kinematic inversion of *Radiguet* [2011].

For our analysis, we separate the SSE sequence into two subevents (SE1 and SE2). The quantitative definition of the two subevents in terms of constitutive relation will be given later, but the snapshots in Figure 2 show clearly their spatiotemporal extension. The subevents roughly correspond to the period before and after the 2010 Maule earthquake. In fact, at the moment of the 2010 Maule earthquake, SE1 seems to have already finished. Then, SE2 starts complementarily in a different place (Figure 2 rows 3 and 4). We calculate the stress evolution over the whole fault plane, but for the following statistical analysis, we restrain our study to regions where the fault slip is larger than 1 cm for either subevent.

3. Results

Figure 2 shows the snapshots of the slip evolution during the 2009–2010 SSE and the corresponding shear stress change calculated from equation (2). The positive and negative changes represent the stress accumulation and release, respectively. The maximum stress variations are the same for both SSEs (approximately 0.1 MPa) as seen on the color scale ($X = -100$ km / $Y = 50$ km for SE1 and $X = 25$ km / $Y = 50$ km for SE2).

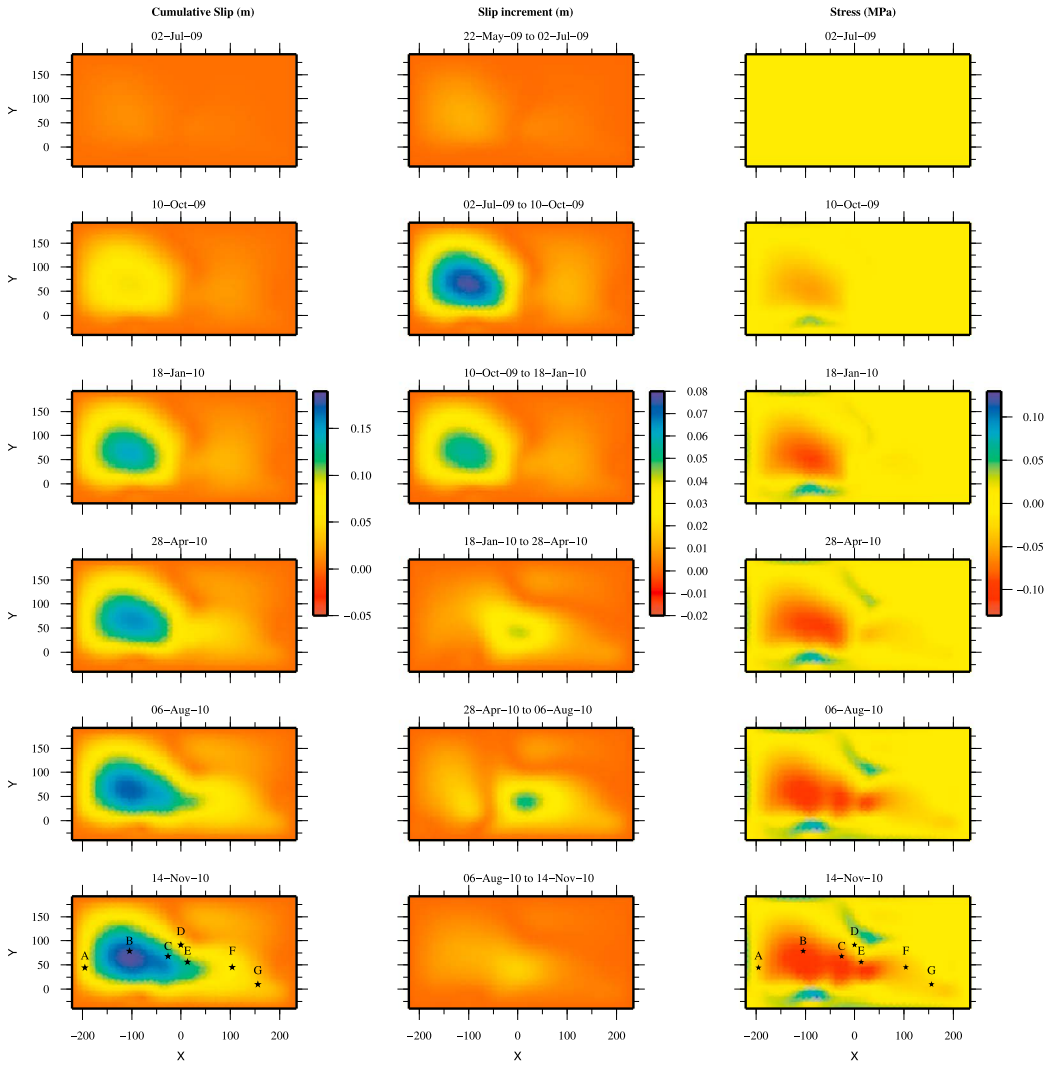

Figure 2. Snapshots of the 2009–2010 SSE in Guerrero, Mexico, every 100 days. (first column) Cumulative slip in meters after *Radiguet* [2011]. (second column) Slip propagation in each period of 100 days. (third column) Calculated stress evolution in megapascals. The location of subfaults used in Figures 3 and 4 are plotted in Figure 2 row 6. The origin of coordinates is centered at Acapulco.

We select several representative points on the fault (A to G) plotted in Figure 2 and show the stress evolution with time in Figure 3a. This stress evolution can be evaluated as a function of slip in Figure 3b. Although there is no constraint on the constitutive relation, we systematically find a linear decrease of stress with the ongoing slip, usually known as linear "slip-weakening."

We define quantitatively the two subevents (SE1 and SE2) based on the constitutive relation in the following way: we seek the local maximum and minimum of the stress function, τ_{max} and τ_{min}, respectively, corresponding to each period for each point. If the extrema are found only once (one subevent is not clear), we check the initiation time of slip. Therefore, this distinction is not exactly separated at the moment of the 2010 Maule earthquake (Figure 3a). Moreover, we attribute a linear decrease of stress with slip to a subevent only if this decrease is longer than 50 days. If it is less than 50 days, we exclude this point considering that the temporal resolution is insufficient for further analysis. For the points B, C, and F, where the slip is large, we clearly find that the shear stress decreases twice with an intermediate stable period before the 2010 Maule earthquake. This suggests that the fault slip is triggered again by the stress perturbation generated by the distant mega-earthquake.

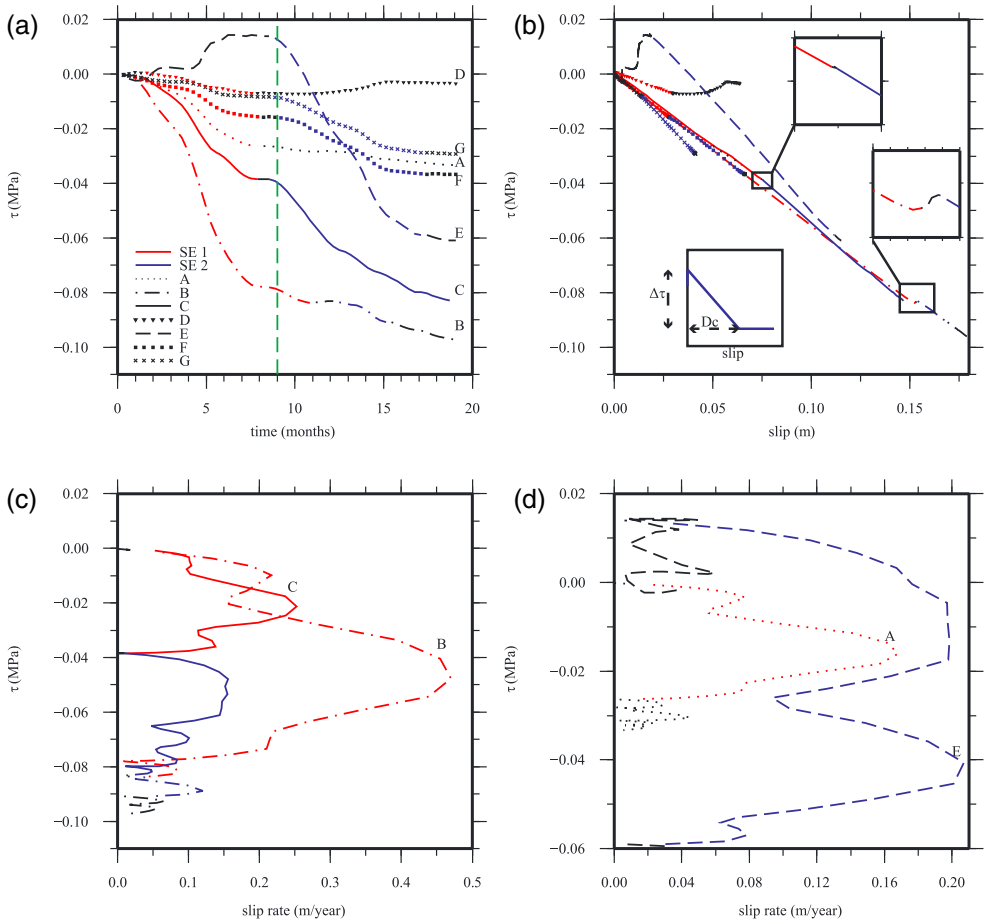

Figure 3. Evolution of the stress as a function of time, slip, and slip rate for seven subfaults (see their positions in Figure 1 or 2). Different colors on the lines indicate the corresponding subevents (SE1 in red, SE2 in blue, and the rest in black. See the definition in text). Subfaults B, C, and F are affected by both subevents, A and D are only affected by SE1, and E and G only by SE2. (a) Stress evolution as a function of time. The green broken line represents the occurrence of the 2010 Maule earthquake. (b) Shear stress as a function of slip. A zoom is made at the beginning of SE2 for two subfaults. A slip-weakening relation (equation (3)) is schematically illustrated in the inset. (c, d) Shear stress as a function of slip rate for the four subfaults.

It is generally admitted that the coseismic dynamic rupture process follows a slip-weakening process [*Ide and Takeo*, 1997] and the following simple expression is mostly adopted:

$$\tau(u) = -\Delta\tau \frac{u}{D_c} + \tau_0 \text{ for } u \le D_c, \tag{3}$$

where $\Delta\tau$ represents the stress drop, τ_0 represents the yield stress, and D_c represents the characteristic slip distance, which may differ from L in equation (1). In the dynamic rupture process, the value of D_c exists with respect to the corresponding $\Delta\tau$, namely, the shear stress has a residual value ($\tau_0 - \Delta\tau$ here) after a point slips more than D_C, and the fracture energy ($\equiv \Delta\tau D_c/2$) is the essential parameter to understand the earthquake scaling [e.g., *Ide and Aochi*, 2005].

However, during the SSEs, no evident D_c is observed, while the slopes are always similar not only for these selected points but also for the whole fault (see Figure S4 in the supporting information). We also notice that the slope itself is unchanged, even after the Maule earthquake. We estimate a mean slope of -0.5 ± 0.2 MPa/m. The mean stress drop during the SSEs (i.e., during each subevent) is about 0.03 MPa, which is much smaller than the stress drop of regular earthquakes (a few MPa), in agreement with the small displacements and large slip area. The mean D_c is estimated to be 6 cm if we regard it as the corresponding distance needed for the stress drop. With these values for D_c and the stress drop, the energy release rate $Gc = D_c\Delta\tau/2$ is estimated to be 1 kJ/m^2 3 orders of magnitude lower than Gc for classical earthquakes

of equivalent magnitude [*Beroza and Spudich*, 1988]. The transition from SE1 to SE2 is hardly visible in the stress-slip relation (Figure 3b) and barely resolved. In the two inset zoom windows, we find a very small increase in stress of approximately 0.7 kPa for point B (i.e., for the biggest increase of the two). The fault is slightly healed by a few kilopascals between the two subevents but conserves the same weakening process continuously without resetting. Point E has a different behavior, it does not follow a slip weakening but a slip-hardening behavior during the SE1. It is only during the second subevent the process becomes slip weakening. This point is located in the region of origin of the second subevent. Initially, it is mainly loaded by the larger slip occurring on adjacent subfaults. The change in frictional behavior is then likely triggered by the dynamic perturbation caused by the Maule earthquake.

We also plot the shear stress change versus slip velocity in Figures 3c and 3d for the four points with the highest stress decrease. As the form of the slip time function is not constrained, there are some perturbations in the velocity (there are several accelerations and decelerations in each subevent). We find no unique relation between the two variables, and no evident strengthening process (except maybe for point E at the beginning). The maximum slip velocity is variable, and in most cases, it is larger in SE1 compared to SE2 simply because SE1 produces larger slip.

4. Discussion

The overall stress evolution can be characterized by a linear slip-weakening relation. This is very similar to the coseismic dynamic rupture process [e.g., *Ide and Takeo*, 1997], regardless of the difference in time scale (we are discussing a scale of months, while the coseismic process is approximately seconds). The weakening slope during the SSE is relatively gradual and lower by an order of magnitude than the weakening slope of coseismic process (less than a MPa/m compared to a few MPa/m). According to the small amount of slip and stress drop, Gc is found smaller by 3 orders of magnitude than the Gc of coseismic process. These differences in behavior are probably caused by different mechanical behavior below the seismogenic zone as well as by the longer time scale of the SSE; namely, the rheology is constantly influenced by healing process. This result most likely occurs because the fault behavior at this depth is more ductile than for a simple brittle failure. The perturbation of the 2010 Maule earthquake does not seem to affect the ongoing slip-weakening evolution. However, the dynamic perturbation may have changed the mechanical behavior for some points. The frictional properties of the eastern part of the fault evolve from slip-hardening to slip-weakening behavior following the Maule earthquake.

The observation of slip hardening as well as the gradual weakening slope is highly suggestive of healing mechanism taking place. This healing process is not included in a simple slip-weakening relation. Therefore, we are wondering if the obtained constitutive relations can be fitted by equation (1) and thus explained by a rate and state law. We fit the stress-slip rate relation curve (Figure 3) to determine the parameters of the rate- and state friction law. We carry out this inversion for the whole duration of both SE1 and SE2 (e.g., from $t11$ the beginning of SE1 to $t22$ the end of SE2) using a single set of parameters. Equation (1) can be rewritten to have only four unknowns ($A = a\sigma_n$, $B = b\sigma_n$, L, and $\tau_* = \mu_*\sigma_n - a\sigma_n lnV_* + b\sigma_n lnV_*$). Following *Bizzarri and Cocco* [2003] for the coseismic case and *Liu and Rice* [2005] for the slow slip modeling, we assume that the initial value θ_0 of the state variable θ corresponds to one of steady state, that is

$$\theta_0 = \frac{L}{V_0} \tag{4}$$

After several tests, we select $V_0 = 0.1$ mm/year in equation (4), corresponding to the stationary convergence rate of this plate interface. We find no significant influence in the results of the inversion (variation of L lower than 5%), even if lower values of V_0 are assumed. The value of V_0 is usually much lower than the slip rate V found in the inversion. During the analysis from $t11$ to $t22$, the slip rate V is large enough ($V \gg 0$).

For a given slip velocity, a grid search is performed to determine the best set of parameters to fit the shear stress evolution. The searched range of each parameter is, respectively $A = [0.001, 0.015]$ MPa, $B = [0.006, 0.1]$ MPa, $L = [0.001, 0.075]$ m, and $\tau_* = [-1, 0]$ MPa. The misfit function χ is evaluated independently for each subfault by the following definition:

$$\chi = \sum_{t11}^{t22} (\tau_{\text{calc}} - \tau_{\text{obs}})^2 \tag{5}$$

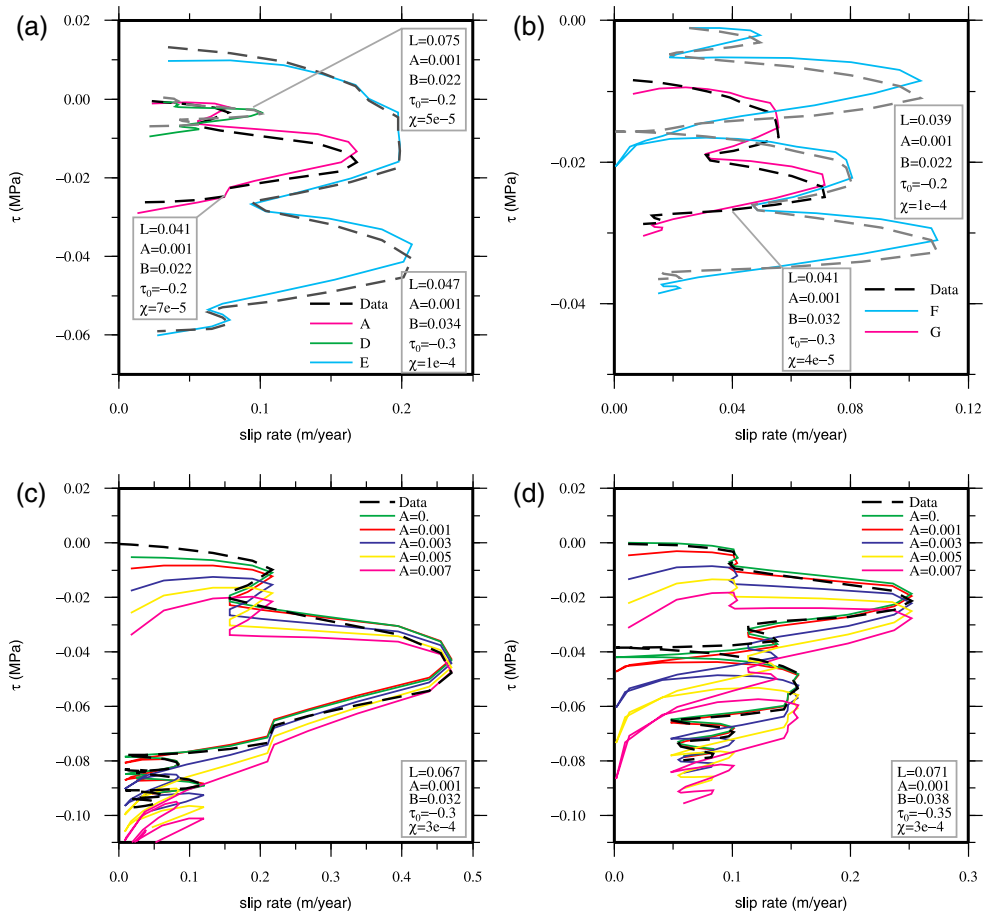

Figure 4. Inversion of the stress evolution to determine the parameters of the rate- and state-dependent friction law for subfaults (a) A, D, and E and (b) F and G. The data are shown by the discontinuous curves in shades of grey. The best parameter set and misfit for each subfault are shown asides. (c, d) Sensitivity test of the parameter A (A=a.σ_n) on the fitting for two subfaults (B in Figure 4c and C in Figure 4d). The more A increases, the less the stress at low slip rate is fit. The best parameters shown in the grey rectangle correspond to the continuous red curve. See the locations of the subfaults in Figures 1 or 2.

A good fit is obtained for most points (Figures 4a and 4b) with a misfit function lower than 10^{-4}. Both subevents are well explained using the same set of parameters. The parameter distribution is heterogeneous (see Figure S5 in the supporting information) but no systematic variation in depth is observed.

From these results (Figure 4), the value of $(B-A)$ is approximately 0.02 MPa. Thus, assuming a value of $(b-a)$ to be 0.004 as commonly used for coseismic process [*Bizzarri and Cocco*, 2003] or slow slip models [*Liu and Rice*, 2005], the value of effective normal stress σ_n (equation (1)) is estimated as 5 MPa. This value is confirmed by consideration on stiffness. As there is no sign of dynamic instability, the stiffness of the system should be lower than the critical stiffness [*Dieterich*, 1992], that is

$$\frac{(b-a)\sigma_n}{L} \leq \frac{2\mu}{3r} \tag{6}$$

where $\mu = 50$ GPa is the shear modulus and $r = 80$ km the radius of the fault patch. Using $L = 5$ cm and $b-a = 0.004$, equation (6) leads to a normal effective stress lower than 5 MPa. Note that these estimations of σ_n depend on the assumed value for $b-a$. These low values of effective normal stress could also be coherent with the ultraslow velocity layer detected in Guerrero [*Song et al.*, 2009].

It is interesting to note that, for any point on the interface, the best fit is always found for $A = 0.001$ (see Figure S5 in the supporting information), which is the lowest value tested. In Figures 4c and 4d, we show a sensitivity test on the parameter A. If A is increased, the stress history at velocities lower than 0.2 m/year is

significantly different from the observations. In contrast, if A is null, a better fit is observed for low velocities. The mean value of the parameter B is 0.02 ± 0.01.

Therefore, $A - B < 0$ and $A \ll B$; that is, the SSE is governed by a velocity weakening regime, and the kinetic (rate) term A is negligible compared to the evolution (state) term B. A small value of A during the SSEs seems different from the feature usually thought for the numerical simulations [*Bizzarri and Cocco*, 2003] (A value of the same order as B).

The mean value of L is found to be 5 cm, nearly equal to the slip amount during the SSE. This value is large compared to the value of 10^{-5} m used in the numerical simulations for classical earthquakes [*Bizzarri and Cocco*, 2003]. L is spatially variable (Figures 4a and 4b), but the value is always on the order of centimeters (variation from 2 cm to 7 cm, see Figure S5 in the supporting information).

5. Conclusion

The Slow Slip Event (SSE) of 2009–2010 Guerrero, Mexico has been studied in terms of stress evolution and fault constitutive relation based on the kinematic inversion result. Without imposing any friction law, a slip weakening behavior is systematically observed over the whole slip area, while no unique relation between shear stress and slip velocity is found. The mean slope of the slip-weakening process (slip-weakening rate) is −0.5 MPa/m, slightly lower than the value known for dynamic rupture process of regular earthquakes. We observe no well constrained value of D_c, e.g., the residual shear stress level. The stress perturbation following the 27 February 2010 Maule, Chile earthquake is small but could trigger the second sequence of the SSE. The constitutive relation remains unchanged before and after the 2010 Maule earthquake. The slip-weakening process, which seems to have stopped before the Mauke earthquake, restarts along the same slip-weakening line. The complex trajectory observed between shear stress and slip velocity can be fitted using a rate and state friction law. The frictional parameters are evaluated through inversion. We obtain $A = 0.001$ MPa, $B = 0.02$ MPa, $L = 5$ cm. The value of A is very small compared to the B value, suggesting that the kinetic effect is negligible. Assuming a $(b - a)$ value of 0.004 as suggested by temperature-dependent experimental observations [*Marone*, 1998], the effective normal stress should be a few megapascals. This low value may be related to the existence of a high pore fluid pressure zone on the subduction. The value of L is bigger than the one of 10^{-5} m assumed for regular earthquakes but coherent with the value used in the modeling of SSEs [*Liu and Rice*, 2005].

In conclusion, the frictional behavior of SSE is very similar to the fault constitutive relation known for regular earthquakes, but with different parameter values. A unified mechanical model should be more quantitatively explored in the future to explain the difference between the weakening process of SSE and regular earthquakes.

Acknowledgments

We thank Jean-Philippe Avouac and Raul Madariaga for their constructive comments and remarks that helped to improve our study. This work has been partially supported by the research project "Subduction Standard and Slow Seismology" through grant ANR-2011-BS56-017 of the French "Agence Nationale de la Recherche". M.R. was funded by the Swiss National Science Foundation (grant PMPDP2_145448). For information on the slip spatiotemporal history contact M.R. We thank people from IG-UNAM, SSN and ISTerre who participated in the GPS network installation and maintenance, as well as the people from ISTerre involved in the GPS data processing.

The Editor thanks Jean-Philippe Avouac and Raul Madariaga for their assistance in evaluating this paper.

References

Beroza, G., and S. Ide (2009), Deep tremors and slow quakes, *Science*, *324*, 1025–1026, doi:10.1126/science.1171231.

Beroza, G., and P. Spudich (1988), Linearized inversion for fault rupture behavior: Application to the 1984 Morgan Hill, California earthquake, *J. Geophys. Res.*, *93*(B6), 6275–6296, doi:10.1029/JB093iB06p06275.

Bizzarri, A., and M. Cocco (2003), Slip-weakening behavior during the propagation of dynamic ruptures obeying rate- and state-dependent friction laws, *J. Geophys. Res.*, *108*(B8), 2373, doi:10.1029/2002JB002198.

Dieterich, J. (1979), Modeling of rock friction: 1. Experimental results and constitutive equations, *J. Geophys. Res.*, *84*(B5), 2161–2168.

Dieterich, J. (1992), Earthquake nucleation on faults with rate- and state-dependent strength, *Tectonophysics*, *211*, 115–134.

Ide, S., and H. Aochi (2005), Earthquakes as multiscale dynamic ruptures with heterogeneous fracture surface energy, *J. Geophys. Res.*, *110*, B11303, doi:10.1029/2004JB003591.

Ide, S., and M. Takeo (1997), Determination of constitutive relations of fault slip based on seismic wave analysis, *J. Geophys. Res.*, *102*(B12), 27,379–27,391.

Kositsky, A., and J.-P. Avouac (2010), Inverting geodetical time series with a principal component analysis-based inversion method, *J. Geophys. Res.*, *115*, B03401, doi:10.1029/2009JB006535.

Liu, Y., and J. Rice (2005), Aseismic slip transients emerge spontaneously in three-dimensional rate and state modeling of subduction earthquake sequences, *J. Geophys. Res.*, *110*, B08307, doi:10.1029/2004JB003424.

Marone, C. (1998), Laboratory-derived friction laws and their application to seismic faulting, *Annu. Rev. Earth Planet. Sci.*, *26*, 643–696.

Peng, Z., and J. Gomberg (2010), An integrated perspective of the continuum between earthquakes and slow-slip phenomena, *Nat. Geosci.*, *3*, 599–607, doi:10.1038/NGEO940.

Radiguet, M. (2011), Etude des seismes lents et du chargement intersismique dans la lacune sismique de Guerrero au Mexique, PhD thesis, Univ. Joseph Fourier at Grenoble, Grenoble, France.

Radiguet, M., F. Cotton, M. Vergnolle, M. Campillo, A. Walpersdorf, N. Cotte, and V. Kostoglodov (2012), Slow slip events and strain accumulation in the Guerrero gap, Mexico, *J. Geophys. Res.*, *117*(B4), B04305, doi:10.1029/2011JB008801.

Shibazaki, B., and T. Shimamoto (2007), Modelling of short-interval silent slip events in deeper subduction interfaces considering the frictional properties at the unstable-stable transition regime, *Geophys. J. Int.*, *171*, 191–205, doi:10.1111/j-1365-246X.2007.03434.x.

Song, T.-R., D. Helmberger, M. Brudzinski, R. Clayton, P. Davis, X. Perez-Campos, and S. Singh (2009), Subducting slab ultra-slow velocity layer coincident with silent earthquake in Southern Mexico, *Science*, *324*, 502–506.

Tada, T., E. Fukuyama, and R. Madariaga (2000), Non-hypersingular boundary integral equations for 3-D non-planar crack dynamics, *Comput. Mech.*, *25*(6), 613–626, doi:10.1007/s004660050508.

Zigone, D., et al. (2012), Triggering of tremors and slow slip events in Guerrero, Mexico, by the 2010 Mw 8.8 Maule, Chile, earthquake, *J. Geophys. Res.*, *117*, B09304, doi:10.1029/2012JB009160.